Microscopic study of ground and low-lying states in neutron-rich ^{103,105,107}Mo isotopes within the quasiparticle-phonon coupling plus rotor model

J. Inchaouh,[1,*] M. K. Jammari,[2] O. Jdair,[1] A. Khouaja,[1] M. L. Bouhssa,[1] H. Chakir,[1] and A. Morsad[1]
[1]*Department of Physics, LPMC-ERSA, Faculty of Sciences Ben M'Sik, Hassan II Mohammedia University, Casablanca, Morocco*
[2]*Department of Physics, Faculty of Sciences Ain chock, Hassan II Casablanca Ain chock University, Casablanca, Morocco*
(Received 12 August 2013; published 2 December 2013)

The band-head systematic ground-state spins and parities of one-quasineutron states along an odd-A Mo isotopic chain are studied by using the quasiparticle-phonon coupling plus rotor model. Within this model, the individual excitation is retained in a deformed Nilsson average field and a monopole pairing interaction from BCS. The vibrational collective motion is derived from the quadrupole phonon term of the Tamm-Dancoff approximation. The two effects of recoil and Coriolis forces are included with the assumption of a symmetric rotational motion. To determine the intrinsic states of an odd nucleus, we have adopted an exact diagonalization in the basis of one-quasiparticle and quasiparticle-phonon states. The structural evolution via the ground and low-lying one-quasineutron states is systematically studied for ^{103,105,107}Mo with comparison to the available experimental data.

DOI: 10.1103/PhysRevC.88.064301 PACS number(s): 21.60.Jz

I. INTRODUCTION

The microscopic structure of neutron-rich nuclei near $A \sim 100$ is of particular interest in studying the effect of nuclear deformation and shape coexistence phenomena of the transitional region. For the even $_{38}$Sr and $_{40}$Zr isotopes, a sudden onset of strong deformation is observed from $N = 60$, whereas, the lighter isotopes up to $N = 58$ are rather spherical [1]. It has been shown for $N = 59$ isotones by using the quasiparticle rotor model (QRM) that some shapes coexist, particularly, the two unique-parity states $\pi g_{9/2}$ and $\nu h_{11/2}$ in the structure of ^{97}Sr, ^{99}Zr, and ^{96}Rb isotopes [1,2]. The clear identification of the band-head spins, their deformations, and the Nilsson orbitals of $N = 59$ isotones have provided new insight for understanding the mechanisms responsible for this rapid change in shapes, which are highlighted from the quadrupole moment measurements of the ground state for Rb isotopes [3].

However, by using the self-consistent total Routhian surface (TRS) model for $N > 59$ isotones, it has been shown that the nuclear structures of $N = 63$ ^{103}Zr and ^{105}Mo isotones have medium triaxiality parameters of $\gamma = 0^\circ$ and $\gamma = -19^\circ$ [4], respectively. The triaxial effect, a sign of strong deformation, is more important for Mo isotopes than for Zr ones by using the rigid triaxial rotor plus particle model and the TRS model [4,5]. Experimentally, by producing Zr and Mo isotopes from fusion-fission reaction mechanisms, the analysis of experimental data performed in the framework of QRM showed that the triaxial degree of freedom is more prominent for Mo than Zr isotopes [6]. In these calculations, the cranked shell model was used for the study of the crossing frequency of the aligned bands. It was concluded that the alignment of the $\nu h_{11/2}$ neutron orbital is responsible for the first band crossing in the even Zr and Mo isotopes [6], which strongly influences the behavior of the $5/2^-[532]$ band head in the odd-Zr and odd-Mo isotopes.

In the transitional region $A \sim 100$, the nuclear shape is known to be soft spherically deformed, which, theoretically, is the reason to not use a rigid triaxiality. It is then better to treat this spherically deformed shape by the coupling between (axial) rotation and vibration. Therefore, in our paper, we have used a microscopic description of the spectroscopy of neutron-rich odd-A = 105 and 133 nuclei [7,8]. We have used a Soloviev [9] inspired model: the quasiparticle phonon plus rotor where a Tamm-Dancoff approximation (TDA) phonon was used instead of a random-phase-approximation one. For the transitional region, a microscopic structure is considered for the quadrupole phonon by means of the TDA, developed in the Ring-Schuck book [10]. This method is microscopic and provides a two-quasiparticle structure of the quadrupole vibrational core (γ phonon) [11] in contrast to the phenomenological model in which the phonon structure is excluded. Already, such structures of 1γ and 2γ bands have been observed in ^{103}Nb, ^{105}Mo, ^{104,106,108}Mo, and ^{108,112}Ru [4,6,12–14] nuclei.

In the present paper, we want to verify the ability of our quasiparticle-phonon coupling plus rotor model (QPRM) predictions in the spectroscopy of odd-A nuclear systems of the transitional region at a very low-energy spectrum within a window less than 1 MeV from the ground-state level. The goal is twofold. First, from an isotonic chain $N = 61$ (^{99}Sr, ^{101}Zr, ^{103}Mo, and ^{105}Ru), we want to study the band head, such as ground and excited states, of a one-quasineutron structure. We study the contribution of different (quadrupole and recoil forces, initial pairing interactions) corrective terms on the intrinsic states. And, when the final result is compared with the available data, the ground state is assigned, and the origin of the excited ones is identified from their corresponding band heads. With the second goal, we want to verify the performance of our predictions in an isotopic chain of ^{103,105,107}Mo. From the evolution of the band-head structure, the spectroscopic

*jamalinch@gmail.com

schemes could be established for this isotopic chain with help from the available experimental data.

This paper is organized as follows. In Sec. II, we present the Hamiltonian formalism that treats the one-quasiparticle system in terms of intrinsic, rotational, and Coriolis motions. For a deformed nucleus system, we retained the dynamical deformation (vibrational excitation) and residual rotational motion in terms of quadrupole and recoil forces. We evaluated the intrinsic state by using, together, the contributions of the Nilsson, BCS, and TDA approximations. In Sec. III, we pay attention to the possible states, which could form the ground state close to the Fermi level. We systematically discuss the evolution structure of the ^{99}Sr, ^{101}Zr, ^{103}Mo, and ^{105}Ru isotonic chains and qualitatively discuss the main features of the observed trends in the ^{103,105,107}Mo isotopic chain. And, finally, we devote our conclusions and perspectives to the ability of our formalism to describe the nuclear structure in the transitional region.

II. THEORITICAL FORMALISM

In the present paper, our calculations are investigated via the QPRM model, which is based on the Nilsson, BCS, and TDA formalisms. The originality of this method could be demonstrated by the diagonalization of the total Hamiltonian, which emanates from individual and collective correlations.

A. The total Hamiltonian formalism

Theoretically, the odd-A nucleus is treated as a system of an extra nucleon coupled to an even-even core with the standard assumption of the total Hamiltonian [15],

$$H = H_{\rm rot} + H_{\rm int}, \tag{1}$$

where $H_{\rm rot}$ is the collective kinetic energy associated with the rotation of the nucleus and $H_{\rm int}$ is the intrinsic motion treated as a one-body deformed potential field H_{sp} plus a two-body residual interaction composed of a short-range constant pairing force H_p and a quadrupole part H_Q of the long-range multipole-multipole force [10].

The kinetic energy of the rotational motion in the laboratory system is developed as

$$H_{\rm rot} = A_1 R_1^2 + A_2 R_2^2 + A_3 R_3^2, \tag{2}$$

where R_k is the component of the collective angular momentum along the axis of intrinsic system. A_k is the corresponding rotational parameter defined as $A_k = \hbar^2/2\Im_k$ with the moment of inertia parameter $\Im_k$ around the three principal axes $k = 1$–3 of the nuclear mass distribution.

In this paper, we limit our analysis to the case of a nucleon coupled to an axially symmetric rotor [16] instead of the general triaxial form presented in Eq. (2). The rotational Hamiltonian can then be reduced to

$$H_{\rm rot} = \hbar^2 \left(R_1^2 + R_2^2\right)/2\Im, \tag{3}$$

with the same moment of inertia $\Im$ along the two axes $k = 1,2$ perpendicular to the symmetry axis $k = 3$.

The total angular momentum I is composed of the two terms: the collective rotation of the core R and the angular momentum of the extra nucleon J; $I = R + J$. Since I is a conserved quantity, R in Eq. (3) is replaced by I and J. The total Hamiltonian of Eq. (1) is then expressed as [16]

$$H = H_{\rm int} + H_I + H_C, \tag{4}$$

where

$$\begin{aligned} H_{\rm int} &= H_{sp} + H_P + H_Q + H_J, \quad H_I = A_R\left(I^2 - I_3^2\right), \\ H_C &= -A_R\left(I_+ J_- + I_- J_+\right), \quad H_J = A_R\left(J^2 - J_3^2\right), \end{aligned} \tag{5}$$

with $I_\pm = I_1 \pm i I_2$, $J_\pm = J_1 \pm i J_2$, and $A_R = \hbar^2/2\Im$.

The total Hamiltonian H is, therefore, separated into three terms, the intrinsic $H_{\rm int}$, rotational H_I, and Coriolis H_C terms which couple the intrinsic and rotational motions. The intrinsic Hamiltonian is more interesting from a physical point of view. It is separated into four parts. The first, H_{sp}, contains the deformed potential field which governs the independent motion of the nucleons. In this sense, we prefer to use the Nilsson harmonic-oscillator model, which is rather simple and more used to describe a deformed nucleus. By using a second quantization, H_{sp} becomes [17]

$$H_{sp} = \sum_{\nu\tau} e_{\nu\tau} a^\dagger_{\nu\tau} a_{\nu\tau}, \tag{6}$$

where $a^\dagger_{\nu\tau}$ ($a_{\nu\tau}$) is the operator that creates (destroys) a particle of nucleon type τ (neutron or proton) in a Nilsson orbital and with an energy $e_{\nu\tau}$. The quantum number ν stands for the asymptotic quantum along numbers [N,n_z,Λ] with the projection Ω_ν of the particle angular momentum along the symmetry axis. The term H_P describes the monopole pairing interaction with the strength parameter G_τ and is written as [15]

$$H_P = -\sum_{\nu\mu\tau} G_\tau a^\dagger_{\nu\tau} a^\dagger_{-\nu\tau} a_{-\mu\tau} a_{\mu\tau}. \tag{7}$$

The next term H_Q is the quadrupole-quadrupole force and is expressed by [10]

$$H_Q = -\frac{1}{2}\chi \sum_{\tau\tau'} \{Q^\dagger_{22}(\tau) Q_{22}(\tau') + Q^\dagger_{2-2}(\tau) Q_{2-2}(\tau')\}, \tag{8}$$

where the quadrupole moment of mass with $\gamma = \pm 2$ is given as a one-body interaction,

$$Q_{2\gamma}(\tau) = \sum_{\nu\tau\mu} \langle \nu\tau | r^2 Y_{2\gamma} | \mu\tau \rangle a^\dagger_{\nu\tau} a_{\mu\tau}. \tag{9}$$

The last term H_J of Eq. (5) is the recoil force. In some earlier papers, H_J was neglected with the argument that it could be absorbed in the independent nucleon motion of the potential average field [15]. Here, we have decided to treat it in the same way as a residual interaction into the intrinsic motion. By using the second quantization, H_J can be expressed as

$$H_J = \frac{1}{2} A_R \sum_{\tau\tau'} [J_+(\tau) J_-(\tau') + J_-(\tau) J_+(\tau')], \tag{10}$$

where the one-body interaction of the intrinsic momentum $J_\pm$ is written as

$$J_\pm(\tau) = \sum_{\nu\tau} \langle \nu\tau | J_\pm | \mu\tau \rangle a^\dagger_{\nu\tau} a_{\mu\tau}. \quad (11)$$

The term H_I of Eq. (4) represents the kinetic energy of rotational motion and reproduces the energy difference between intrinsic states in a rotational band. The inclusion of Coriolis force H_C requires the matrix of the Hamiltonian model H to be constructed and diagonalized within the space of symmetrized functions [15],

$$|IMK_\rho\rangle = \sqrt{\frac{2I+1}{16\pi^2}} \left\{ D^I_{MK} |K_\rho\rangle + (-)^{I+K} D^I_{M-K} |\overline{K_\rho}\rangle \right\}. \quad (12)$$

Here, ρ is the quantum number of a given intrinsic state with a projection K of the intrinsic angular momentum along the symmetry axis. $|K_\rho\rangle$ can be obtained by resolving the secular problem,

$$H_{\rm int}|K_\rho\rangle = (H_{sp} + H_P + H_Q + H_J)|K_\rho\rangle = E^{\rm int}_{K_\rho}|K_\rho\rangle. \quad (13)$$

As is well known, D^I_{MK} is the rotational matrix and is an eigenfunction of I^2 and I^3 with respective eigenvalues $I(I+1)$ and K. To diagonalize H within the basis states, therefore, Eq. (12) essentially requires determining the matrix element of the Coriolis term H_C [16],

$$\begin{aligned} &\langle IMK'_{\rho'}|H_C|IMK_\rho\rangle \\ &= -A_R \left\{ (-)^{I+1/2} \left(I + \frac{1}{2}\right) \langle K'_{\rho'}|J_+|\overline{K_\rho}\rangle \delta_{K'1/2}\delta_{K1/2} \right. \\ &\left. + \sqrt{(I \mp K)(I \pm K + 1)} \langle K'_{\rho'}|J_\pm|\overline{K_\rho}\rangle \delta_{K',K\pm1} \right\}. \quad (14) \end{aligned}$$

To summarize, from the above equations, we note that such systems should be processed in two steps. First, the intrinsic eigenvalue of Eq. (13), when solved, gives a set of intrinsic states $|K_\rho\rangle$ and intrinsic energies $E^{\rm int}_K$. From these states, different rotational wave functions with the form given in Eq. (12) are constructed. Then in a second step, a diagonalization of the Coriolis term is performed.

B. Intrinsic Hamiltonian formalism

To discuss the different terms of Eq. (13) and their intrinsic eigenvalue, we first have to look to the possible combinations of the system. By neglecting H_J and H_Q, we have a model which describes the independent nucleon motion in a Nilsson deformed potential and to which are added the pairing correlations. The BCS approximation is adopted so as to transform the system to an independent quasiparticle motion. The long-range interaction of quadrupole type H_Q is introduced in a sense to take the dynamical mode of deformation and/or the vibrational excitation into account. We work in the frame of the Tamm-Dancoff approximation to build a microscopic structure description for the γ-phonon state. Furthermore, in this case, the intrinsic Hamiltonian will contain a residual part of the rotational motion by retaining the recoil force H_J, which is independent in regard to the total angular momentum I. The BCS method is an approximate approach to the treatment of pairing correlation by using the Bogoliubov-Valatin transformation that makes the change from particle to quasiparticle operators [18],

$$a^\dagger_{\sigma\nu\tau} = U_{\nu\tau}\alpha^\dagger_{\sigma\nu\tau} + \sigma V_{\nu\tau}\alpha_{-\sigma\nu\tau}. \quad (15)$$

Here, the operator $\alpha^\dagger_{\sigma\nu\tau}$ ($\alpha_{\sigma\nu\tau}$) creates (destroys) a quasiparticle state $|\sigma\nu\tau\rangle$ with a σ sign that depends on time-reversal symmetry and where the occupational (nonoccupational) probability is expressed by $U_{\nu\tau}$ ($V_{\nu\tau}$). The expression deduced from $H_{sp} + {\rm H}_P$ is given by

$$H_{\rm BCS} = T + \sum_{\sigma\nu\tau} E_{\nu\tau}\alpha^\dagger_{\sigma\nu\tau}\alpha_{\sigma\nu\tau}, \quad (16)$$

where T is the BCS ground-state energy and $E_{\nu\tau}$ is the energy of a single quasiparticle,

$$E_{\nu\tau} = \sqrt{\left(e_{\nu\tau} - \lambda - G_\tau V^2_{\nu\tau}\right)^2 + \Delta^2_\tau}, \quad (17)$$

where λ is the Lagrange multiplier and Δ_τ is the energy gap.

In the same way, the transformation in Eq. (15) allows the expression of quadrupole [Eq. (9)] and intrinsic [Eq. (11)] moments to be translated into the form of quasiparticle terms,

$$\begin{aligned} Q_{2\gamma}(\tau) = &\sum_{\sigma\sigma'=\pm1,\nu\nu'} G^{\gamma,\tau}_{\sigma\nu\sigma'\nu'}\alpha^\dagger_{\sigma\nu\tau}\alpha_{\sigma'\nu'\tau} \\ &- \frac{1}{2}\sum_{\sigma\sigma'=\pm1,\nu\nu'} \left(\sigma' F^{\gamma,\tau}_{\sigma\nu-\sigma'\nu'}\alpha^\dagger_{\sigma\nu\tau}\alpha^\dagger_{\sigma'\nu'\tau} \right. \\ &\left. + \sigma F^{\gamma,\tau}_{-\sigma\nu\sigma'\nu'}\alpha_{\sigma\nu\tau}\alpha_{\sigma'\nu'\tau}\right), \quad (18) \end{aligned}$$

where

$$G^{\gamma,\tau}_{\sigma\nu\sigma'\nu'} = (U_{\nu\tau}U_{\nu'\tau} - V_{\nu\tau}V_{\nu'\tau})\langle\sigma\nu\tau|r^2Y_{2\gamma}|\sigma'\nu'\tau\rangle, \quad (19)$$

$$F^{\gamma,\tau}_{\sigma\nu\sigma'\nu'} = (U_{\nu\tau}U_{\nu'\tau} + V_{\nu\tau}V_{\nu'\tau})\langle\sigma\nu\tau|r^2Y_{2\gamma}|\sigma'\nu'\tau\rangle, \quad (20)$$

and

$$\begin{aligned} J_\pm(\tau) = &\sum_{\sigma\sigma'=\pm1,\nu\nu'} M^{\pm,\tau}_{\sigma\nu\sigma'\nu'}\alpha^\dagger_{\sigma\nu\tau}\alpha_{\sigma'\nu'\tau} \\ &- \frac{1}{2}\sum_{\sigma\sigma'=\pm1,\nu\nu'} \left(\sigma' N^{\pm,\tau}_{\sigma\nu-\sigma'\nu'}\alpha^\dagger_{\sigma\nu\tau}\alpha^\dagger_{\sigma'\nu'\tau} \right. \\ &\left. - \sigma N^{\pm,\tau}_{-\sigma\nu\sigma'\nu'}\alpha_{\sigma\nu\tau}\alpha_{\sigma'\nu'\tau}\right). \quad (21) \end{aligned}$$

Here,

$$M^{\pm,\tau}_{\sigma\nu\sigma'\nu'} = (U_{\nu\tau}U_{\nu'\tau} + V_{\nu\tau}V_{\nu'\tau})\langle\sigma\nu\tau|J_\pm|\sigma'\nu'\tau\rangle, \quad (22)$$

$$N^{\pm,\tau}_{\sigma\nu\sigma'\nu'} = (U_{\nu\tau}U_{\nu'\tau} - V_{\nu\tau}V_{\nu'\tau})\langle\sigma\nu\tau|J_\pm|\sigma'\nu'\tau\rangle. \quad (23)$$

By introducing these new expressions in Eqs. (8) and (10), respectively, the quadrupole and recoil forces can be decomposed in the form $H_{00} + H_{11} + H_{20} + H_{22} + H_{31} + H_{40}$ where the subscripts refer to the number of quasiparticle creation and annihilation operators. In this form, we notice that both one-body and two-body interactions should be considered [10]. In the frame of the Tamm-Dancoff approximation, the creation operator of the γ phonon is defined as

$$A^\dagger_\gamma = \frac{1}{2}\sum_{\nu\mu\tau} \left(X^\tau_\gamma\right)_{\nu\mu}\alpha^\dagger_{\nu\tau}\alpha^\dagger_{\mu\tau}. \quad (24)$$

This expression allows a microscopic structure description for the quadrupole vibrational core (γ-phonon state) by showing the X amplitudes related to two-quasiparticle excitations.

C. Intrinsic eigenvalue for odd-A nuclei

The solution of Eq. (13) for an odd-A nucleus is perfected by a diagonalization within the basis formed by one-quasiparticle states $(1-qp)$ and quasiparticle-phonon coupling states $(qp-ph_\gamma)$. If we only retain the terms without a zero matrix element, the intrinsic Hamiltonian then is reduced to

$$H_{\rm int} = H_{\rm BCS} + H_{11}^{Q} + H_{20}^{Q} + H_{22}^{Q} + H_{31}^{Q} + H_{11}^{J} + H_{20}^{J} + H_{22}^{J} + H_{31}^{J} + H_{22}^{\prime p}. \quad (25)$$

The Q and J terms are related to quadrupole and recoil forces, respectively. The last term $H_{22}^{\prime p}$ is a residual pairing interaction, which was neglected in the BCS approximation. The interaction between two $1-qp$ and two $qp-ph_\gamma$ states is given by L_{11} and L_{22} matrix elements and that between $1-qp$ and $qp-ph_\gamma$ states by L_{31}, respectively. They are written as follows [19]:

$$L_{11} = \langle {\rm BCS}|\alpha_{K'\tau}\big(H_{\rm BCS} + H_{11}^{Q} + H_{11}^{J}\big)\alpha_{K\tau}^{\dagger}|{\rm BCS}\rangle, \quad (26)$$

$$L_{22} = \langle {\rm BCS}|A_{\gamma'}\alpha_{K'\tau}\big(H_{\rm BCS} + H_{11}^{Q} + H_{11}^{J} + H_{22}^{Q} + H_{22}^{J} + H_{22}^{\prime p}\big)\alpha_{K\tau}^{\dagger}A_{\gamma}^{\dagger}|{\rm BCS}\rangle, \quad (27)$$

and

$$L_{31} = \langle {\rm BCS}|A_{\gamma}\alpha_{K'\tau}\big(H_{20}^{Q} + H_{20}^{J} + H_{31}^{Q} + H_{31}^{J}\big)\alpha_{K\tau}^{\dagger}|{\rm BCS}\rangle. \quad (28)$$

The eigenvalue problem is expressed in matrix form

$$\begin{pmatrix} L_{11} & L_{31} \\ L_{31} & L_{22} \end{pmatrix}\begin{pmatrix} C_K^{\rho} \\ D_{K\gamma}^{\rho} \end{pmatrix} = E_{K_\rho}^{\rm int}\begin{pmatrix} C_K^{\rho} \\ D_{K\gamma}^{\rho} \end{pmatrix}, \quad (29)$$

where C_K^{ρ} represents the $1-qp$ component; the same as $D_{K\gamma}^{\rho}$ for the $qp-ph_\gamma$ component. The intrinsic eigenvalue $E_{K_\rho}^{\rm int}$ corresponds to the eigenvector,

$$|K\rangle = \left(\sum_{\nu} C_{\nu}^{\rho}\delta_{K\Omega_\nu}\alpha_{\nu\tau}^{\dagger} + \sum_{\nu\tau} D_{\nu\gamma}^{\rho}\delta_{K=\Omega_\nu+\gamma}\alpha_{\nu\tau}^{\dagger}A_{\gamma}^{\dagger}\right)|{\rm BCS}\rangle. \quad (30)$$

The overlap between the $1-qp$ and the $qp-ph_\gamma$ states is always zero. However, the overlap between two different $qp-ph_\gamma$ states can be nonzero such that they can form a nonorthogonal basis set,

$$S_{ij} = \langle i|j\rangle = \langle {\rm BCS}|A_{\gamma'}\alpha_i\alpha_j^{\dagger}A_{\gamma}^{\dagger}|{\rm BCS}\rangle = S_{ij}\delta_{\gamma'\gamma} - \sum_{\lambda}(X_{\gamma'})_{j\lambda}(X_{\gamma})_{i\lambda}, \quad (31)$$

where $|i\rangle$ is the $qp-ph_\gamma$ states. To solve this rather eigenvaluelike problem, we adopted the method where we first solve the eigenvalue equation for the S_{ij} overlapping matrix,

$$\sum_j S_{ij}\omega_j^h = n_h\omega_i^h. \quad (32)$$

The eigenvectors obtained can be written in the basis $\{|i\rangle\}$ as

$$|\tilde{i}\rangle = \frac{1}{\sqrt{n_h}}\sum_i \omega_i^h|i\rangle. \quad (33)$$

They have the characteristic to be mutually orthogonal in which they are normalized and form a complete set. The amplitude $D_{\nu\gamma}^{\rho}$ in Eq. (30) then is calculated from the g amplitudes in the following way:

$$D_{\nu\gamma}^{\rho} = \sum_h \frac{1}{\sqrt{n_h}}g_h^{\rho}\omega_\nu^h. \quad (34)$$

III. DISCUSSION

The theoretical method developed in this paper is applied for the transitional region $A\sim 100$ with a particular investigation of the band heads, such as the ground and excited states of ^{103,105,107}Mo, which are treated as a system of an even-even core plus an extra nucleon. It is developed in respect to the following steps: Nilsson, BCS, and TDA calculations. For the Nilsson calculations, the even-even core structure is reproduced by using, conjointly, the deformation parameter ε_2 from Möller *et al.* [20] and Meyer *et al.* data [21] and the $K = 0.068$ and $\mu = 0.35$ parameters of the deformed average Nilsson field. The BCS pairing is fixed for protons and neutrons by the well-known phenomenological relation $\Delta_p = \Delta_n = 12/A^{1/2}$ MeV [22]. For the TDA calculations, the parameter of quadrupole force χ is fitted from the experimental energy of the quadrupole vibrational core by using the experimental data from Refs. [6,14], where ^{102}Mo, ^{104}Mo, and ^{106}Mo have $E(2^+) = 295$, $E(2^+) = 192$, and $E(2^+) = 171$ keV, respectively. The effects of all these parameters are summarized in a subroutine that diagonalizes the total Hamiltonian and where the inertia parameters are determined semiempirically by using the energy of the first excited state $\varepsilon_2^2 \approx 1176[A^{7/3}E(2^+)]^{-1}$ [23,24].

A. Single-particle energies within the Nilsson formalism

According to the deformed shell model, the collective bands—band heads—of the nuclei of interest should originate from single-neutron configurations. In the regions of $28\leqslant Z\leqslant 50$ and $50\leqslant N\leqslant 82$, we search for the band assignments from the calculated Nilsson diagram. As shown in Fig. 1, the single-particle energy is presented as a function of the deformation parameter (ε_2) with pairing correlation parameters $G_p = 19.6A^{-1}$ and $G_n = [19.6 - 15.7(N-Z)A^{-1}]A^{-1}$ MeV, obtained phenomenologically [25]. For the neutron-rich nuclei ^{103,105,107}Mo, localized in the region of deformation parameters ε_2 between 0.3 and 0.4, the collective bands should originate from the $\nu d_{5/2}$, $\nu g_{7/2}$, $\nu s_{1/2}$, and $\nu h_{11/2}$ subshells [26,27]. Therefore, with our Nilsson calculations, we could expect near the Fermi level—candidates to be the ground

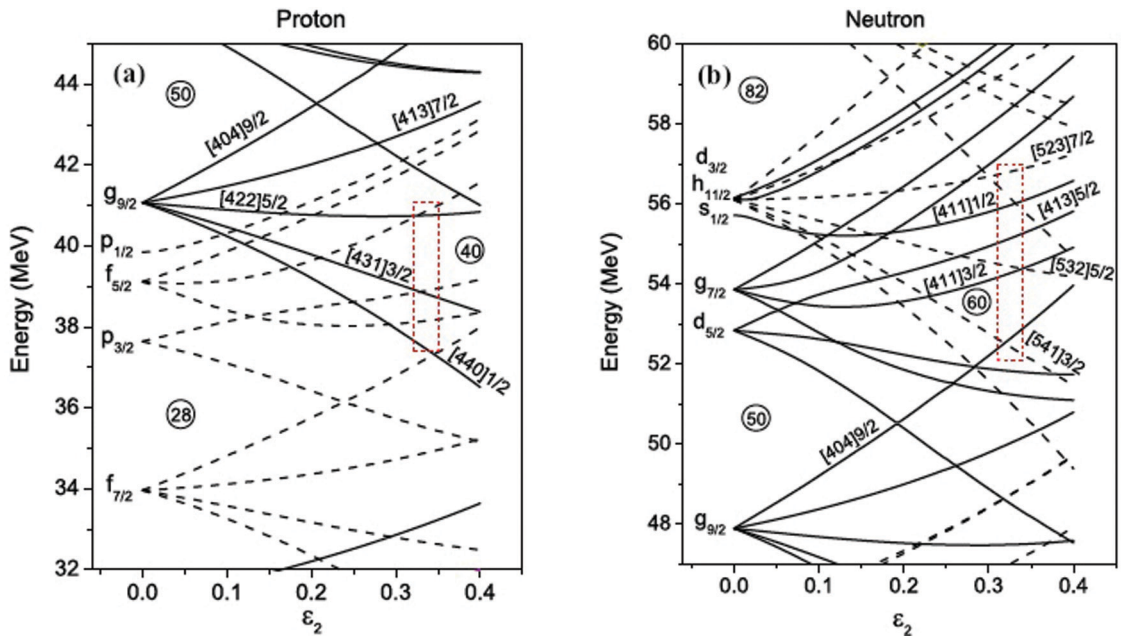

FIG. 1. (Color online) Partial Nilsson diagram for the region of neutron-rich nuclei for (a) with $28 \leqslant Z \leqslant 50$ and (b) with $50 \leqslant N \leqslant 82$.

state—a configuration of single-neutron states built on $1/2^+$, $3/2^+$, $9/2^+$, $1/2^-$, $3/2^-$, $5/2^-$, $5/2^+$, $7/2^-$, and $9/2^-$. Thereby, the assembly of these states will help us in the study and assignment of collective bands observed at low energy in ^{103,105,107}Mo. In the following, we first demonstrate the ability of our method in studying the collective bands of ^{103}Mo, which will be treated as a system of the even-even core of ^{102}Mo plus an extra nucleon.

B. One-quasiparticle states in ^{103}Mo within the BCS formalism

For ^{103}Mo, where the ^{102}Mo core is localized with a deformation parameter of $\varepsilon_2 = 0.3$, we have to primarily identify the ground state from the excited ones in a region where the excitation gap is more important with regard to the deformation parameter. We introduced the BCS method in which the correlation probability between quasiparticle operators (creation and annihilation) is well determined. With

TABLE I. Quasiparticle energy levels calculated for ^{102}Mo (neutron cases) around the Fermi surface.

Band-head number	Band-head levels	Energy levels (MeV)	U	V
21	$5/2^+[422]$	5.959	0.100	0.995
22	$5/2^-[303]$	4.772	0.125	0.992
23	$1/2^-[301]$	4.749	0.126	0.992
24	$1/2^+[431]$	4.367	0.137	0.990
25	$7/2^+[413]$	3.814	0.158	0.987
26	$1/2^+[420]$	2.429	0.252	0.967
27	$1/2^-[550]$	2.043	0.305	0.952
28	$3/2^+[422]$	2.013	0.310	0.950
29	$9/2^+[404]$	1.559	0.419	0.907
30	$3/2^-[541]$	1.385	0.493	0.870
		Fermi level		
31	$3/2^+[411]$	1.342	0.856	0.517
32	$5/2^-[532]$	1.514	0.900	0.436
33	$5/2^+[413]$	1.865	0.941	0.338
34	$1/2^+[411]$	2.579	0.971	0.237
35	$7/2^-[523]$	3.159	0.981	0.191
36	$1/2^-[541]$	3.634	0.986	0.166
37	$5/2^+[402]$	3.855	0.988	0.156
38	$7/2^+[404]$	4.741	0.992	0.126
39	$1/2^-[530]$	5.231	0.993	0.114
40	$9/2^-[514]$	5.382	0.992	0.111

TABLE II. BCS eigenvalues for Nilsson orbitals of ^{102}Mo.

$\langle\nu\|$	$\langle\nu'\|$	$E(\nu)+E(\nu')$
$5/2^+[422]$	$7/2^+[413]$	9.774
$5/2^+[422]$	$3/2^+[422]$	7.972
$5/2^+[422]$	$3/2^+[411]$	7.301
$5/2^+[422]$	$7/2^+[404]$	10.701
$5/2^-[303]$	$3/2^-[541]$	6.157
$-1/2^-[301]$	$1/2^-[301]$	9.498
$-1/2^-[301]$	$1/2^-[550]$	6.792
$1/2^-[301]$	$3/2^-[541]$	6.134
$-1/2^-[301]$	$1/2^-[541]$	8.383
$-1/2^-[301]$	$1/2^-[530]$	9.980
$-1/2^+[431]$	$1/2^+[431]$	8.734
$-1/2^+[431]$	$1/2^+[420]$	6.797
$1/2^+[431]$	$3/2^+[422]$	6.379
$1/2^+[431]$	$3/2^+[411]$	5.709
$-1/2^+[431]$	$1/2^+[411]$	6.947
$7/2^+[413]$	$9/2^+[404]$	5.373
$7/2^+[413]$	$5/2^+[413]$	5.679
$7/2^+[413]$	$5/2^+[402]$	7.669
$-1/2^+[420]$	$1/2^+[420]$	4.859
$1/2^+[420]$	$3/2^+[422]$	4.442
$1/2^+[420]$	$3/2^+[411]$	3.771
$-1/2^+[420]$	$1/2^+[411]$	5.009
$-1/2^-[550]$	$1/2^-[550]$	4.086
$1/2^-[550]$	$3/2^-[541]$	3.428
$-1/2^-[550]$	$1/2^-[541]$	5.677
$-1/2^-[550]$	$1/2^-[530]$	7.274
$3/2^+[422]$	$5/2^+[413]$	3.878
$3/2^+[422]$	$1/2^+[411]$	4.592
$3/2^+[422]$	$5/2^+[402]$	5.868
$9/2^+[404]$	$7/2^+[404]$	6.300
$3/2^-[541]$	$5/2^-[532]$	2.899
$3/2^-[541]$	$1/2^-[541]$	5.019
$3/2^-[541]$	$1/2^-[530]$	6.616
$3/2^+[411]$	$5/2^+[413]$	3.207
$3/2^+[411]$	$1/2^+[411]$	3.922
$3/2^+[411]$	$5/2^+[402]$	5.197
$5/2^-[532]$	$7/2^-[523]$	4.674
$5/2^+[413]$	$7/2^+[404]$	6.607
$7/2^-[523]$	$9/2^-[514]$	8.541

this method, we numerically treat an energy of 10 up and down band-head levels for ^{103}Mo—candidates to be the ground state—around the Fermi level. In Table I, with a precision of 10^{-7} after seven iterations, for each subsequent level, we present the calculated eigenenergies and their occupancy (U) and vacancy (V) probabilities. So, when looking for the closest energy level to the Fermi one, we could have a confusing decision if one treats and finds the ground state only according to its energy level. In Table II, we carried out the whole possible ground and excited states correlated from the particular states presented in Table I. The combinations between states (columns 1 and 2) are treated in the approximation of the quasiparticle-independent model where the Hamiltonian is as follows: $H = U_0 + \sum_{\mu\nu}(E_\mu + E_\nu)\alpha^\dagger_\mu\alpha_\nu$, and the correspondent energy is presented in column 3. We find three possible combinations of states. With the lowest energy $(E_\mu + E_\nu)$ according to the Fermi level, the ground state could be formed from the couple $(3/2^-[541],5/2^-[532])$ with an energy level of 2.899 MeV, the couple $(1/2^-[550],3/2^-[541])$ with 3.428 MeV, or the couple $(1/2^+[420],3/2^+[411])$ with 3.771 MeV. Therefore, when comparing these eigenvalues with the ones from Table I, we could expect one of the $5/2^-[532]$, $3/2^-[541]$, and $3/2^+[411]$ orbitals to be the ground state of ^{103}Mo.

C. One-quasiparticle states in ^{103}Mo within the TDA formalism

In the TDA, ^{103}Mo could be treated in a simple way as a two-body interaction where the shape softness of ^{102}Mo could be introduced in a dynamic manner by γ vibration [see Eq. (24)]. In Table III, we carried out the amplitude values $(X_\gamma)_{\mu\nu}$ of the TDA phonon for the different combinations of states around the Fermi level. From this table and with respect to the possible combinations found with the TDA formalism, we find that state $3/2^+[411]$ presents the largest vibration -0.296 compared to the nearest ones of -0.213 and -0.189 for $5/2^-[532]$ and $3/2^-[541]$, respectively. Consequently, in the approximation of the quasiparticle-phonon coupling model, we adopted the $3/2^+[411]$ orbital, which originated from the $\nu g_{7/2}$ subshell, to be the ground state of ^{103}Mo, which is in good agreement with the experimental assignment from Refs. [6,28].

D. One-quasiparticle states in ^{103}Mo within the QPRM formalism

In Fig. 2, we show the contribution of each term of the intrinsic Hamiltonian [Eq. (25)] to the energy of the intrinsic states, assigned by the dominant one-quasiparticle configuration, and which are positioned close to the Fermi level. The dashed lines connect the states characterized by the same asymptotic quantum numbers $\Omega^\pi[N,n_z,\Lambda]$, where Ω is the quantum number that corresponds to the third component of the angular momentum in the intrinsic frame, π and N are its parity and the principal quantum number of the major oscillator shell, n_z is the number of quanta associated with the wave function moving along the z direction, and Λ is the projection of the orbital angular momentum onto the z axis (symmetry axis).

Here, as we can see by adding the quadrupole and recoil forces to the pairing interaction, the spectroscopy scheme at low energy could be adjusted and could be compared to the available experimental data from Refs. [6,28]. We note that, with the quadrupole force, both one-body and two-body terms exhibit an important interaction for positive-parity states by looking at their energy levels that decrease rapidly. The same behavior is observed when the recoil force effect is added to the previous one. Both forces show an important influence on the neutron states that belong to the $N = 4$ oscillator shell, strongly mixed by deformation [30]. We see that the $1/2^+[411]$, $3/2^+[422]$, and $5/2^+[413]$ intrinsic states, which originate from the $\nu s_{1/2}$ and $\nu d_{5/2}$ subshells, interchange their energy-level positions. According to the discussion in Ref. [30], the neutrons in the region of interest occupy the states that belong to the $N = 4$ shell and begin to fill the $\nu h_{11/2}$ intruder orbitals from $N = 5$. These intruder orbitals polarize the core towards large deformations (oblate or prolate), and

TABLE III. TDA calculations for neutron structures in ^{102}Mo. X is the amplitude of each couple of orbitals. Each couple is identified by the excitation energy $E_\nu + E_{\nu'}$ and the quadrupole moment of mass. $F_{\nu\nu'}$ and $G_{\nu\nu'}$ are the quadrupole coefficients.

$\langle\nu\vert$	$\vert\nu'\rangle$	$E_\nu + E_{\nu'}$	$\langle\nu\vert r^2 Y_{22}\vert\nu'\rangle$	$F_{\nu\nu'}$	$G_{\nu\nu'}$	X
$3/2^+[422]$	$1/2^+[431]$	6.379	−0.122	0.438	−0.899	0.010
$3/2^+[422]$	$1/2^+[420]$	4.442	0.952	0.540	−0.841	−0.142
$3/2^+[422]$	$1/2^+[411]$	4.592	−0.141	0.997	0.076	0.037
$3/2^-[541]$	$1/2^-[301]$	6.134	−0.003	0.598	−0.801	−0.001
$3/2^-[541]$	$1/2^-[550]$	3.428	−0.703	0.735	−0.678	−0.189
$3/2^-[541]$	$1/2^-[541]$	5.019	0.589	0.939	0.342	0.134
$3/2^-[541]$	$1/2^-[530]$	6.616	−0.149	0.921	0.390	−0.025
$3/2^+[411]$	$1/2^+[431]$	5.709	0.249	0.919	−0.395	−0.049
$3/2^+[411]$	$1/2^+[420]$	3.771	−0.039	0.959	−0.284	0.012
$3/2^+[411]$	$1/2^+[411]$	3.922	1.328	0.705	0.709	−0.296
$5/2^+[422]$	$1/2^+[431]$	10.327	0.387	0.236	−0.972	0.010
$5/2^+[422]$	$1/2^+[420]$	8.389	−0.855	0.348	−0.937	−0.042
$5/2^+[422]$	$1/2^+[411]$	8.539	0.069	0.990	−0.138	0.009
$5/2^-[303]$	$1/2^-[301]$	9.521	−1.195	0.249	−0.968	−0.037
$5/2^-[303]$	$1/2^-[550]$	6.815	0.001	0.422	−0.906	0.000
$5/2^-[303]$	$1/2^-[541]$	8.406	0.013	0.999	−0.041	0.002
$5/2^-[303]$	$1/2^-[530]$	10.003	0.012	0.999	0.011	0.001
$7/2^+[413]$	$3/2^+[422]$	5.827	0.366	0.456	−0.889	0.035
$7/2^+[413]$	$3/2^+[411]$	5.156	−1.115	0.927	−0.376	−0.244
$9/2^+[404]$	$5/2^+[422]$	7.518	−0.225	0.509	−0.861	−0.018
$9/2^+[404]$	$5/2^+[413]$	3.424	0.269	0.996	0.088	0.098
$9/2^+[404]$	$5/2^+[402]$	5.414	−1.359	0.962	0.273	−0.293
$5/2^-[532]$	$1/2^-[301]$	6.263	−0.003	0.948	−0.319	−0.001
$5/2^-[532]$	$1/2^-[550]$	3.557	−0.612	0.990	−0.140	−0.213
$5/2^-[532]$	$1/2^-[541]$	5.148	0.388	0.579	0.815	0.053
$5/2^-[532]$	$1/2^-[530]$	6.745	−0.825	0.536	0.844	−0.079
$5/2^+[413]$	$1/2^+[431]$	6.232	−0.261	0.978	−0.206	−0.049
$5/2^+[413]$	$1/2^+[420]$	4.2945	−0.003	0.996	−0.089	−0.009
$5/2^+[413]$	$1/2^+[411]$	4.445	−1.177	0.552	0.834	−0.179
$7/2^-[523]$	$3/2^-[541]$	4.545	−0.518	0.948	0.317	−0.132
$5/2^+[402]$	$1/2^+[431]$	8.222	0.023	0.999	−0.019	0.003
$5/2^+[402]$	$1/2^+[420]$	6.285	−0.183	0.995	0.099	−0.035
$5/2^+[402]$	$1/2^+[411]$	6.435	0.073	0.386	0.923	0.005
$7/2^+[404]$	$3/2^+[422]$	6.754	−0.187	0.982	0.188	−0.033
$7/2^+[404]$	$3/2^+[411]$	6.083	−0.012	0.621	0.784	−0.002
$9/2^-[514]$	$5/2^-[303]$	10.154	−0.008	0.999	0.014	−0.001
$9/2^-[514]$	$5/2^-[532]$	6.896	−0.396	0.533	0.846	−0.037

as a consequence, the underlying nuclear structure is very sensitive to the occupancy of these single-particle orbitals. We then have a configuration of $N = 5$ for states $3/2^-[541]$ and $5/2^-[532]$ that originate from the $\nu h_{11/2}$ subshell, $N = 4$ for states $1/2^+[411]$ and $3/2^+[411]$ that originate from $\nu g_{7/2}$, $3/2^+[422]$ and $5/2^+[413]$ that originate from $\nu d_{5/2}$, $1/2^+[411]$ that originates from $\nu s_{1/2}$, and finally, $9/2^+[404]$ that originates from the $\pi g_{9/2}$ subshell. Consequently, the energy-level configuration is more improved when the pairing effect is added, and then the ground state has an energy level close to the Fermi level, which corresponds to the experimentally observed ground state [6,28]. Our theoretical results (the excited states referred to as the corresponding ground states) are plotted in comparison to the experimental ones below the 1-MeV energy window of the plot. The ground state found in our calculations is assigned to be $3/2^+[411]$, which rises from $\nu g_{7/2}$, which is in good agreement with the experimental assignment. As discussed in Refs. [6,28], ^{103}Mo has an excited state at 346.6 keV, assigned to be $5/2^-[532]$. By looking at the result of our calculations, this state, localized at 349.0 keV, is well predicted to originate from the $\nu h_{11/2}$ orbital. According to Refs. [6,28], the first excited state $5/2^+$ is positioned at 102.6 keV, which, in our calculations, may correspond to the excited state $5/2^+[413]$ that comes from the $\nu d_{5/2}$ orbital. To fix such observations, it is interesting to study the isotonic behavior of the considered odd-A nucleus ^{103}Mo where we expect to observe a very similar spectroscopic scheme in the neighboring nuclei (isotones with $N = 61$).

E. One-quasiparticle isotonic systematic trend $N = 61$

In Fig. 3, we investigate the isotonic chain of $N = 61$ (^{99}Sr, ^{101}Zr, ^{103}Mo, and ^{105}Ru) by our QPRM model by using

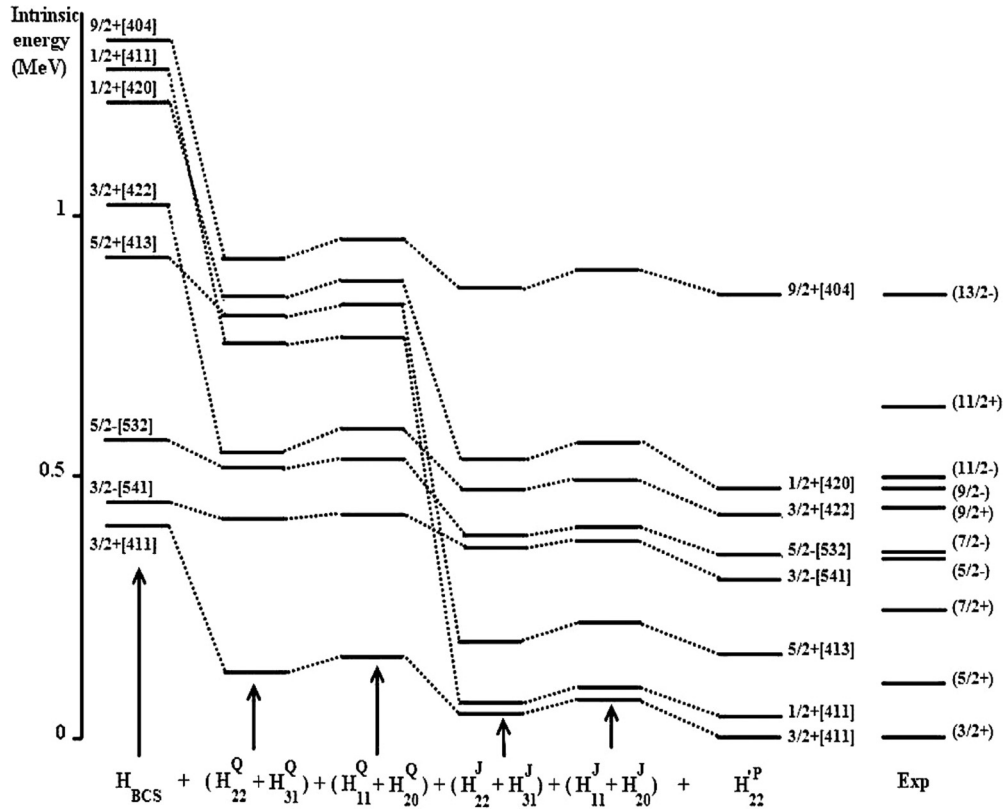

FIG. 2. Intrinsic states of ^{103}Mo that show the contribution of different terms of quadrupole, recoil forces, and the initial pairing interaction.

the deformation parameters given by Möller *et al.* [20]. For each given isotope, the excited states are referred to as the corresponding ground state. Along this isotonic chain, they are connected (characterized) by their asymptotic quantum numbers $[N,n_z,\Lambda]\Omega^{\pi}$. We compare our predicted results with the experimental ones of the low-lying one quasineutron from Refs. [28,30–33]. As we can see, the ground state is well reproduced at $3/2^+[411]$. In Refs. [31–33], the level scheme has been adopted for ^{99}Sr, ^{101}Zr, and ^{105}Ru. An assignment of $5/2^-[532]$ was suggested from the systematic of the neighboring nuclei. It appears at $E = 423.3$ keV for ^{99}Sr, $E = 216.67$ and 673.52 keV for ^{101}Zr, and at $E = 246.37$, 587.0 and 644.03 keV for ^{105}Ru. Within the framework of our calculations, we localize this state at $E = 626$, 558, 349, and 661 keV for ^{99}Sr, ^{101}Zr, ^{103}Mo, and ^{105}Ru, respectively. In the same way, the first $5/2^+$ excited state is observed at $E = 102.56$ and 107.94 keV in ^{103}Mo and ^{105}Ru, respectively. By our calculations, it is plotted at $E = 161$ and 99 keV as originating from $\nu d_{5/2}$ for both isotopes. We also plot the evolution of the $1/2^+$ excited state observed at $E = 159.52$ keV for ^{105}Ru and localized by our calculations at $E = 181$ keV to be raised from $\nu s_{1/2}$. Meanwhile, at this stage of the paper, it appears premature to compare our predictions in terms of excited energy. The idea, however, is to track the structural evolution of the ground and excited one-quasiparticle states along the considered isotonic chain.

The originality of these results for the isotonic chain (^{99}Sr, ^{101}Zr, ^{103}Mo, and ^{105}Ru) helps us to further study the systematic of the Mo isotopes (^{103,105,107}Mo), which are the most difficult to analyze [6,30] and where the blocking effects of the $\nu h_{11/2}$ bands are dominant.

F. One-quasiparticle isotopic systematic trend in ^{103,105,107}Mo

According to the discussions in Refs. [4,6,30,33,34], the rotational bands of the lowest quasiparticle states in ^{105}Mo and ^{107}Mo are measured. For ^{105}Mo, a yrast band, built on the $5/2^-[532]$ Nilsson orbital plus five collective bands, is shown. Among them, three positive-parity bands were proposed to be built on the $3/2^+[411]$, $5/2^+[413]$, and $1/2^+[411]$ Nilsson orbitals based on the 246.3-, 310.0-, and 332.0-keV levels, respectively. This level scheme is redistributed for ^{107}Mo where the ground state is proposed to be built on the $5/2^+[413]$ Nilsson orbital. The other excited states $1/2^+$, $3/2^+$, and $5/2^-$ are tentatively assigned and are proposed at 65.4, 66.0, and 66.3 keV, respectively. However, such observations of the γ-vibrational collective band structure, the high-spin state of $5/2^-[532]$, in odd-A Mo isotopes are treated by using the TRS model and a medium triaxiality shape [29,30] for ^{105}Mo with $\gamma \sim -19^\circ$ [4,26] are shown. Within the cranked shell model, the blocking effects of the $\nu h_{11/2}$ bands in the odd-Mo isotopes indicate that the $h_{11/2}$ neutron alignment is responsible for the first band crossings in the even-Mo isotopes. However, as a first step, to show this dominance in ^{105}Mo, we performed Nilsson calculations for ^{104}Mo with $\varepsilon_2 = 0.317$. As presented in Table IV and around the Fermi level, there are many positive-parity and negative-parity states that originate from $1f_{5/2}$, $2p_{1/2}$, $1g_{9/2}$, $2d_{5/2}$, $1g_{7/2}$, $3s_{1/2}$, and $1h_{11/2}$ Nilsson

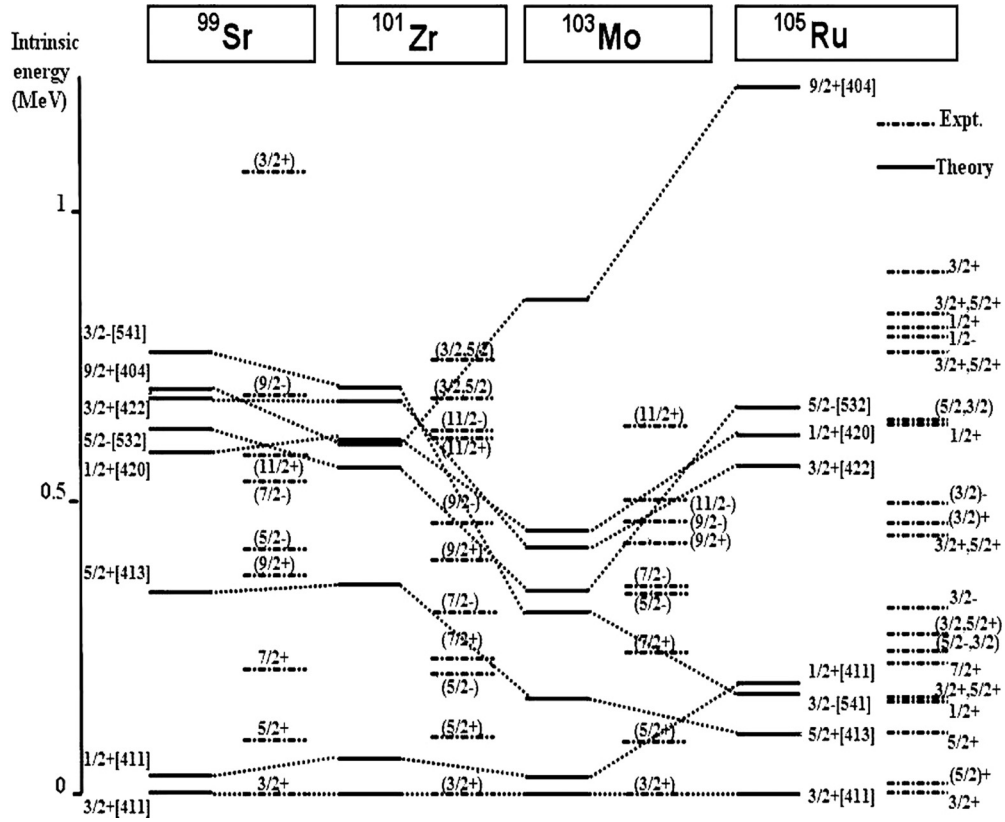

FIG. 3. Experimental excitation energies and spin-parity assignments of the noncollective states compared with the QPRM results for the isotonic chain $N = 61$. The dashed lines follow the states characterized by the same asymptotic quantum numbers $\Omega^{\pi}[N,n_z,\Lambda]$.

orbits with equal occupancy probability, candidates for the ground state of ^{105}Mo. Among them, we have a mixture of four band heads $5/2^-[532]$, $3/2^+[411]$, $5/2^+[413]$, and $1/2^+[411]$ very close to the Fermi level according to the eigenvalues of the Nilsson Hamiltonian. In fact, the low-lying states of ^{105}Mo are built on the correlation of the core particle ^{104}Mo plus the neutron of valence. If one takes the strong Coriolis effect for high-spin state $5/2^-[532]$ into account when approaching the deformation parameter $\varepsilon_2 \sim 0.3$, we could expect a dominance of the $\nu h_{11/2}$ bands in the structure of odd ^{105}Mo.

In Fig. 4, the structural evolution of the ground and one-quasiparticle excited states along the considered Mo isotopic chain (^{103,105,107}Mo) can be followed in comparison to the experimental data from Refs. [4,6,30,33,34] by looking at the dashed lines that connect the states characterized by the same asymptotic quantum numbers $\Omega^{\pi}[N,n_z,\Lambda]$. Our QPRM calculations provide us with the observed $1/2^+$, $3/2^+$, $5/2^+$, and $5/2^-$ one-quasiparticle configurations in odd Mo. They nicely reproduce the ground $5/2^+[413]$ and excited $5/2^-[532]$ states in ^{107}Mo. On the other hand, the experimental configuration is completely interchanged for ^{105}Mo. We obtain the ground $5/2^+[413]$ state and the sequence of excited ones $5/2^-[532]$, $1/2^+[411]$, and $3/2^+$ [411] localized at 63-, 145-, and 169-keV energy levels. This discrepancy with the experimental observations could be explained by our limited study on the low-lying states in terms of a soft spherically deformed shape. As we can see from Fig. 5, for an odd nucleus, the specific features of the low-energy states are determined by the orbital of the odd nucleon [35]. The total spin I is built as the sum of the spin of the odd particle J and the collective spin of the core R, which is built from all the paired nucleons.

According to the strength of I, we could have two extreme excitation (coupling) forms of the nucleus: deformed [Fig. 5(a)] or rotational [Fig. 5(b)] alignments. In our calculations, we adopted the first case to describe the collective bands in odd-A Mo isotopes. Then, it was found that, for such an orbital in a deformed axially symmetric potential, in addition to parity, only the projection of the angular momentum J on the symmetry axis Ω is a preserved quantum number. The rotational collective energy of an axially symmetric nucleus, around a symmetry axis, is calculated from Eq. (5) as

$$H_{\rm rot} = R^2/2\Im = 1/2\Im[(I_1 - J_1)^2 + (I_2 - J_2)^2] = 1/2\Im\left[I^2 - I_3^2 + \left(J_1^2 + J_2^2\right) - (I_+J_- + I_-J_+)\right]. \quad (35)$$

The term $(I_+J_- + I_-J_+)$ corresponds classically to the Coriolis (centrifugal) force, which describes the coupling between the motion of the particle in the deformed potential and the collective rotation. For a small I, this term is treated in first-order perturbation theory where the influence of the rotational motion of the intrinsic structure of the nucleus can be neglected and can be referred to as an adiabatic approximation or a strong-coupling limit.

The selection rules for J_+ and J_- are $\Delta\Omega = \pm 1$, and each orbital of the deformed potential is twice degenerated

TABLE IV. Nilsson energy levels and Coriolis-mixing amplitude for neutron intrinsic states in ^{105}Mo near the Fermi level.

Nilsson orbitals	Energy particle ($\hbar\omega$)	Asymptotic Nilsson components (with corresponding spherical orbitals)					
		[402]($2d_{3/2}$)	[411]($1g_{7/2}$)	[422]($2d_{5/2}$)		[431]($1g_{9/2}$)	
$3/2^+$[411]	5.710	−0.176	0.918	0.299		−0.189	
$3/2^+$[422]	5.416	0.182	−0.136	0.838		0.497	
		[400]($2d_{3/2}$)	[411]($3s_{1/2}$)	[420]($1g_{7/2}$)	[431]($2d_{5/2}$)	[440]($1g_{9/2}$)	
$1/2^+$[411]	5.902	−0.141	0.893	0.345	−0.217	−0.125	
$1/2^+$[420]	5.381	0.177	−0.205	0.797	0.531	−0.093	
$1/2^+$[431]	5.139	−0.057	0.296	−0.130	0.661	0.674	
		[402]($1g_{7/2}$)	[413]($2d_{5/2}$)	[422]($1g_{9/2}$)			
$5/2^+$[413]	5.742	−0.108	0.928	0.356			
$5/2^+$[422]	4.969	0.155	−0.334	0.930			
$5/2^+$[402]	6.046	0.971	0.225	−0.081			
		[404]($1g_{7/2}$)		[413]($1g_{9/2}$)			
$7/2^+$[404]	6.150	0.974		0.225			
$7/2^+$[413]	5.193	−0.225		0.974			
		[404]($1g_{9/2}$)					
$9/2^+$[404]	5.504	1.000					
		[503]($2f_{5/2}$)	[512]($1h_{9/2}$)	[523]($2f_{7/2}$)	[532]($1h_{11/2}$)		
$5/2^-$[532]	5.694	−0.064	0.279	−0.380	0.879		
		[301]($2p_{1/2}$)	[310]($1f_{5/2}$)	[321]($2p_{3/2}$)	[330]($1f_{7/2}$)		
$1/2^-$[301]	5.135	0.953	0.297	−0.050	−0.039		
		[503]($1h_{9/2}$)	[514]($2f_{7/2}$)	[523]($1h_{11/2}$)			
$7/2^-$[523]	5.936	0.151	−0.306	0.940			
		[303]($1f_{5/2}$)		[312]($1f_{7/2}$)			
$5/2^-$[303]	5.118	0.966		0.258			
		[505]($1h_{9/2}$)		[514]($1h_{11/2}$)			
$9/2^-$[514]	6.204	−0.201		0.980			
		[501]($3p_{1/2}$)	[510]($2f_{5/2}$)	[521]($3p_{1/2}$)	[530]($1h_{9/2}$)	[541]($2f_{7/2}$)	[550]($1h_{11/2}$)
$1/2^-$[541]	5.953	0.057	−0.120	0.375	−0.157	0.522	0.737
$1/2^-$[550]	5.411	−0.034	0.129	−0.267	0.495	−0.537	0.613
$1/2^-$[530]	6.156	−0.060	0.326	−0.183	0.725	0.479	−0.318
		[501]($3p_{1/2}$)	[512]($1h_{9/2}$)	[521]($3p_{1/2}$)	[532]($1h_{11/2}$)	[541]($1h_{11/2}$)	
$3/2^-$[541]	5.518	0.046	−0.137	0.374	−0.466	0.789	

($\Omega = \pm 1/2$). Thus, for the odd particles, the diagonal matrix elements of the $(I_+J_- + I_-J_+)$ term are different from zero. The K projection of the total angular momentum on the nuclear symmetry axis is a preserved quantum number, and for no collective component, it is $\Omega = K$. On the other hand, the matrix elements $(J_1^2 + J_2^2)$, the recoil term, depend only on the particle wave functions. This means that they are constant for one rotational band. We first consider situations where they are rather small as a first approximation, and we neglect them [35,36] for leading to a configuration with "two odd particles." According to the extreme coupling scheme in Fig. 5, for high spin $\nu h_{11/2}$ bands, the Coriolis term decouples the nucleons of valence from the rotational collective motion of the core [Fig. 5(b)]. This blocking effect favors the break of pairing effect of even-Mo isotopes and then delays the band crossing of the $\nu h_{11/2}$ bands. It is the reason why the $5/2^-$[532] band head that originates from $\nu h_{11/2}$ does not represent the fall to be the ground state of ^{105}Mo.

Finally, as we can see from Fig. 4, the systematic trend of the ground and low-lying states for ^{103,105,107}Mo is calculated within the framework of the QPRM model, and the intrinsic states $3/2^+$[411] and $5/2^+$[413], except for the case of ^{105}Mo where the ground state is $5/2^-$[532], are well reproduced for ^{103}Mo and ^{107}Mo, respectively. They emanate from the

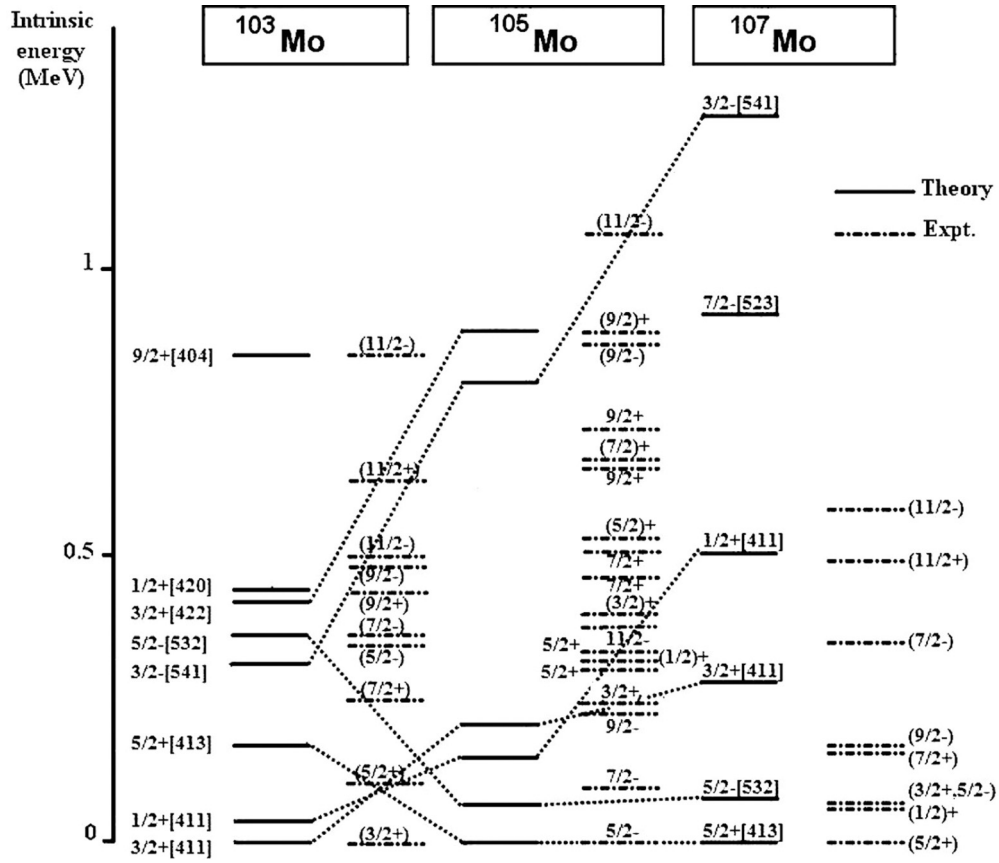

FIG. 4. Systematic of one-quasiparticle states in ^{103,105,107}Mo isotopes, compared to the existing data from Refs. [4,6,30,33,34].

spherical shell $\nu g_{7/2}$ for $3/2^+[411]$ as well as from $\nu d_{5/2}$ for $5/2^+[413]$. Otherwise, for the case of negative parity, our calculations predict the existence of two intrinsic states $3/2^-[541]$ and $5/2^-[532]$, which originate from the $\nu h_{11/2}$ spherical orbital. Their trend indicates an abrupt change in position at $N = 63$. For the nucleus ^{103}Mo, state $3/2^-[541]$ has a lower energy than $5/2^-[532]$. This situation is reversed for the isotopes ^{105}Mo and ^{107}Mo where the energy gap between these two states grew. This effect is explained in terms of the deformation parameter, which varies from $\varepsilon_2 = 0.3$ for ^{103}Mo to $\varepsilon_2 = 0.317$ for ^{105}Mo and 0.325 for ^{107}Mo. Moreover, our results are completely interchanged in ^{105}Mo. This could be explained by our manner of only diagonalizing the total Hamiltonian for low-spin orbitals. Furthermore, our study of the low-lying states of ^{103,105,107}Mo should mutually take into account the two cases shown in Fig. 5. Our work along this line is still in progress and will be reported elsewhere.

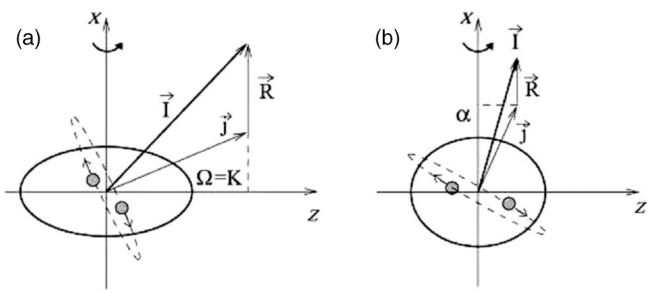

FIG. 5. Schematic of the two extreme coupling schemes: (a) deformed alignment and (b) rotational alignment.

IV. CONCLUSIONS

To summarize, the trend of collective bands, band heads in neutron-rich Mo-odd isotopes, has been studied at low energy within the QPRM, inspired from the microscopic quasiparticle-phonon model of the Soloviev model. We have first used this approach to study the isotonic trends, the ground and low-lying one-quasiparticle configurations of ^{99}Sr, ^{101}Zr, ^{103}Mo, and ^{105}Ru. We have shown that the observed spectroscopic properties have been adjusted from a competition between a quadrupole and the pairing forces. The quadrupole force tends to deform the nucleus (γ softness) in such a situation where the spherical shape is stabilized by the pairing force. When more nucleons are added to the spherical shape (closed shell), the relative strength of the quadrupole force increases, and at a certain point, the transition to the deformed shape takes place. To understand such effects, we have then qualitatively studied the isotopic trends for ^{103,105,107}Mo. We easily reproduced the ground and some low-lying states of ^{103}Mo and ^{107}Mo. On the other hand, it was too complicated to reproduce the ground state of ^{105}Mo, which is owed to the blocking effects of the $\nu h_{11/2}$ bands.

The underlying configuration is interchanged and could be explained in our manner of diagonalizing the total Hamiltonian that favors the deformation alignment. We conclude from these calculations that the study of the high-spin state behavior of the $5/2^-[532]$ bands in the odd-Mo isotopes requires a diagonalization of the total Hamiltonian for both rotational and deformed alignments. There, the rotational alignment favors states with negative parity, and the deformed one favors states with positive parity. Then, we are aware of the challenge to reproduce, in detail, the observed spectroscopic properties of the particular mass region considered in the present study. Nevertheless, our spectroscopic levels scheme at low excitation energy for ^{103,105,107}Mo can be considered as a plausible step forward to a much more detailed paper, which is in progress.

ACKNOWLEDGMENTS

The authors would like to thank Professor A. Cunsolo, Professor F. Cappuzzello, Dr. M. Cavallaro (LNS Catania), and Dr. J. S. Winfield (GSI Darmstadt) for reading, generously offering advice, and suggesting improvements in the content of this paper.

[1] W. Urban *et al.*, Nucl. Phys. A **689**, 605 (2001).
[2] J. A. Pinston *et al.*, Phys. Rev. C **74**, 064304 (2006).
[3] G. Georgiev *et al.*, CERN Report No. CERN-INTC-2009-019/INTC-P-266, IS493, 2009 (unpublished).
[4] H. B. Ding *et al.*, Phys. Rev. C **74**, 054301 (2006).
[5] R. Orlandi *et al.*, Phys. Rev. C **73**, 054310 (2006).
[6] H. Hua *et al.*, Phys. Rev. C **69**, 014317 (2004).
[7] O. Jdair, J. Inchaouh, M. K. Jammari, and H. Chakir, Int. J. Acad. Res. **3**, 1014 (2011).
[8] A. Boulal, J. Inchaouh, and M. K. Jammari, Eur. Phys. J. A **7**, 317 (2000).
[9] V. G. Soloviev, *Theory of Complex Nuclei* (Pergamon, Oxford, UK, 1976).
[10] P. Ring and P. Schuck, *The Nuclear Many-Body Problem* (Springer-Verlag, Berlin, 1980).
[11] M. K. Jammari *et al.*, Nucl. Phys. A **487**, 77 (1988).
[12] J. G. Wang *et al.*, Phys. Lett. B **675**, 420 (2009).
[13] A. Guessous *et al.*, Phys. Rev. Lett. **75**, 2280 (1995).
[14] A. Guessous *et al.*, Phys. Rev. C **53**, 1191 (1996).
[15] A. Bohr and B. R. Mottelson, *Nuclear Structure* (Benjamin, New York, 1975), Vol. 2.
[16] J. M. Eisenberg and W. Greiner, *Nuclear Models* (Elsevier, New York, 1970), Vol. 1.
[17] J. P. Boisson *et al.*, Nucl. Phys. A **168**, 385 (1971).
[18] W. Ogle *et al.*, Rev. Mod. Phys. **43**, 424 (1971).
[19] A. Boulal, A. Zaafa, J. Inchaouh, and M. K. Jammari, *7th International Conference on Nucleus-Nucleus Collisions (NN2000), Strasbourg, France, 2000* (IUPAP, London, 2000).
[20] P. Möller *et al.*, At. Data Nucl. Data Tables **59**, 185 (1995).
[21] R. A. Meyer *et al.*, Nucl. Phys. A **439**, 510 (1985).
[22] P. Möller *et al.*, Nucl. Phys. A **536**, 20 (1992).
[23] L. Grodzins *et al.*, Phys. Lett. **2**, 88 (1962).
[24] F. S. Stephens *et al.*, Phys. Rev. Lett. **29**, 438 (1972).
[25] C. M. Petrache *et al.*, Phys. Rev. C **53**, R2581 (1996).
[26] M. Liang *et al.*, Z. Phys. A **340**, 223 (1991).
[27] Y.-X. Liu *et al.*, Nucl. Phys. A **858**, 11 (2011).
[28] D. De Frenne, Nucl. Data Sheets **110**, 2081 (2009).
[29] R. Rodriguez-Guzman, P. Sarriguren, L. M. Robledo, and S. Perez-Martin, Phys. Lett. B **691**, 202 (2010).
[30] R. Rodriguez-Guzman, P. Sarriguren, and L. M. Robledo, Phys. Rev. C **82**, 044318 (2010).
[31] E. Browne and J. K. Tuli, Nucl. Data Sheets **112**, 275 (2011).
[32] J. Blachot, Nucl. Data Sheets **83**, 1 (1998).
[33] D. De Frenne and E. Jacobs, Nucl. Data Sheets **105**, 775 (2005).
[34] J. Blachot, Nucl. Data Sheets **109**, 1383 (2008).
[35] S. G. Nilsson and I. Ragnarsson, *Shapes and Shells in Nuclear Structure* (Cambridge University Press, Cambridge, UK, 1995), p. 84.
[36] J. Skalski *et al.*, Nucl. Phys. A **617**, 282 (1997).